ACS APPLIED MATERIALS & INTERFACES

www.acsami.org

Research Article

Electrochromic Devices Based on 2D MoO_{3-x}/PEDOT:PSS Composite Film with Boosted Ion Transport

Haolin Yu, Huajing Fang,* Kai Jing, Hailong Ma, Lingqi Wu, and Yang Chai

Cite This: *ACS Appl. Mater. Interfaces* 2024, 16, 18052−18062

Read Online

ACCESS | Metrics & More | Article Recommendations | Supporting Information

ABSTRACT: Electrochromic materials allow for optical modulation and have attracted much attention due to their bright future in applications such as smart windows and energy-saving displays. Two-dimensional (2D) molybdenum oxide nanoflakes with combined advantages of high active specific surface area and natural layered structure should be highly potential candidates for electrochromic devices. However, the efficient top-down preparation of 2D MoO_3 nanoflakes is still a huge challenge and the sluggish ionic kinetics hinder its electrochromic performance. Herein, we demonstrated a feasible thiourea-assisted exfoliation procedure, which can not only increase the yield but also reduce the thickness of 2D MoO_{3-x} nanoflakes down to a few nanometers. Furthermore, electrophoretic-deposited MoO_{3-x} nanoflakes were combined with poly(3,4-ethylenedioxythiophene):poly(styrenesulfonate) (PEDOT:PSS)-conjugated polymer to simultaneously enhance the ionic kinetics and electronic conductivity, with a diffusion coefficient of 3.09×10^{-10} cm^2 s^{-1} and a charge transport resistance of 33.7 Ω. The prepared 2D MoO_{3-x}/PEDOT:PSS composite films exhibit improved electrochromic performance, including fast switching speed (7 s for bleaching, 5 s for coloring), enhanced coloration efficiency (87.1 cm^2 C^{-1}), and large transmittance modulation (ΔT = 65%). This study shows outstanding potential for 2D MoO_{3-x} nanoflakes in electrochromic applications and opens new avenues for optimizing the ion transport in inorganic−organic composites, which will be possibly inspired for other electrochemical devices.

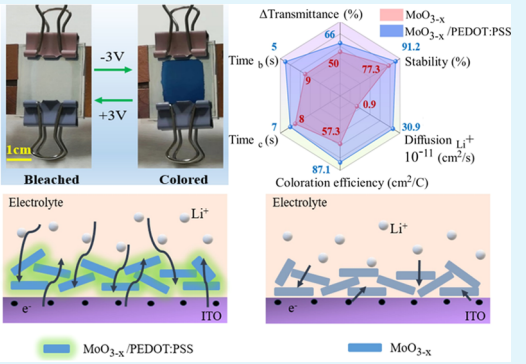

KEYWORDS: *molybdenum oxides, liquid-exfoliated 2D nanoflakes, PEDOT:PSS, electrochromic device, ion transport*

INTRODUCTION

Electrochromic materials have caused immense interest because of their extensive applications including smart windows, information displays, optical camouflage, and so on.[1−3] This kind of functional materials can change their color and optical absorption smartly due to the electrochemical process under an extra applied potential.[4−6] Among a large number of materials studied for electrochromic devices, metal oxides including molybdenum oxides (MoO_3), tungsten oxides (WO_3), and others are based on a similar working mechanism. That is, the reversible electrochemical reaction triggered by the double injection or extraction of cations and electrons.[7−9] Until now, WO_3 is still the main inorganic material studied in the electrochromic field, even though MoO_3 is commercially available and generally less expensive than WO_3. Moreover, MoO_3 also has numerous potential advantages over WO_3 in specific aspects. For example, MoO_3 is nearly 35% less dense than WO_3 (4.7 vs 7.2 g cm^{-3}), allowing for lightweighting and subsequent energy savings in automotive and aerospace applications. The absorption spectrum of MoO_3 in a colored state more closely matches the sensitivity of the human eye than that of WO_3 material.[10,11] However, MoO_3 has not been abundantly researched compared with WO_3. One direct reason is their electrochromic performance is usually inferior to WO_3 under the same conditions.[12] Hence, it is urgent to develop a high-performance electrochromic device based on molybdenum oxides.

Among all of the different crystalline phases of molybdenum oxides, the stable orthorhombic phase (α-MoO_3) with unique chemical and physical properties enables diverse applications such as sensors, catalysts, and nano-optics.[13−16] As a natural layered material, the van der Waals gap inside the architecture allows for small-scale cation intercalation, which has received great attention in the field of electrochemical energy storage.[17−20] However, restricted by the stringent transmittance requirements of smart windows, the general bulk α-MoO_3 material cannot be directly used in the electrochromic field. The ultrathin flake structure makes two-dimensional α-MoO_3 nanomaterials an ideal candidate for electrochromic materials with intrinsic high transparency and high specific surface area. Unfortunately, different from graphene and

Received: January 19, 2024
Revised: March 15, 2024
Accepted: March 19, 2024
Published: March 28, 2024

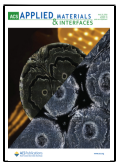

https://doi.org/10.1021/acsami.4c01108
ACS Appl. Mater. Interfaces 2024, 16, 18052−18062

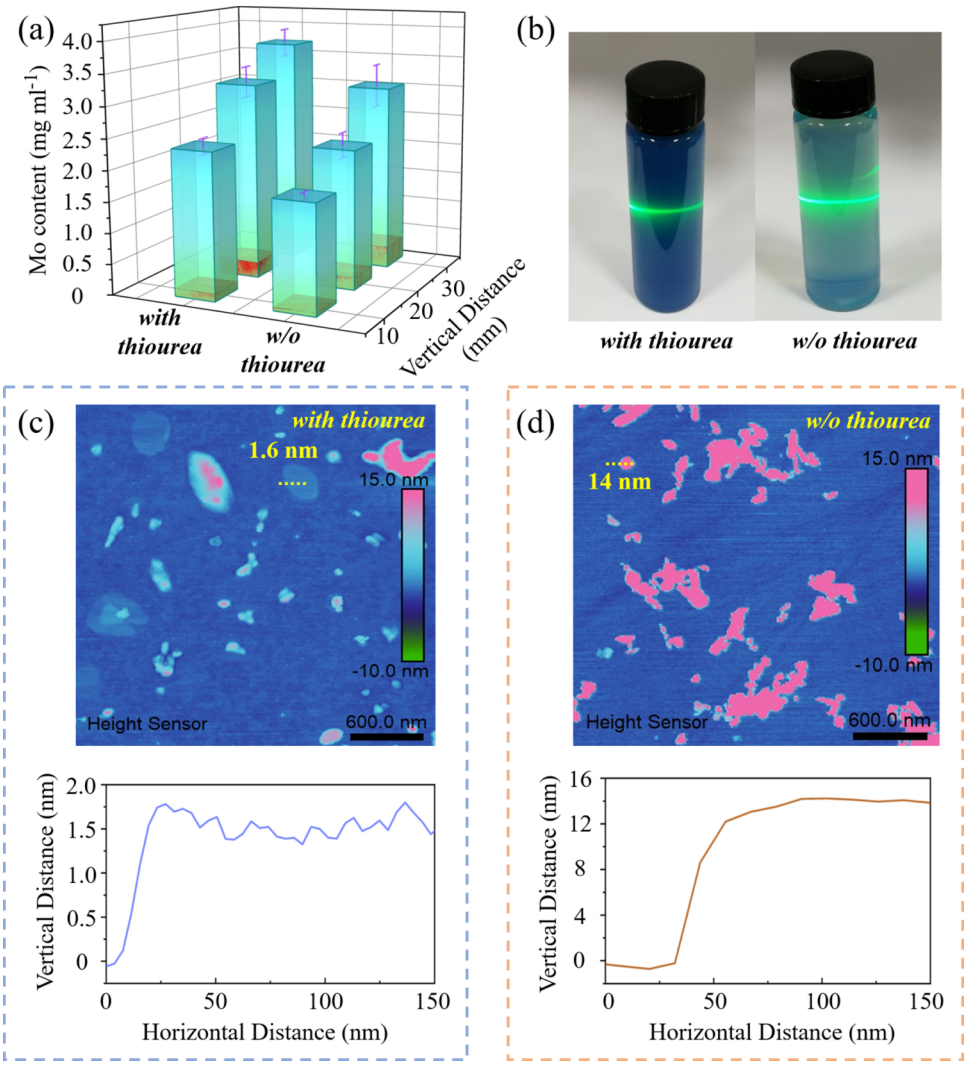

Figure 1. (a) ICP/OES results of the Mo content with error bar. (b) The photograph of MoO_{3-x} nanoflakes supernatants with and without thiourea. (c) Atomic force microscopy (AFM) image and height profile of the thiourea-assisted exfoliated MoO_{3-x} nanoflakes on a sapphire substrate. (d) AFM image and height profile of the MoO_{3-x} nanoflakes without thiourea on a sapphire substrate.

transition-metal dichalcogenides, most transition-metal oxides are difficult to directly exfoliate into two-dimensional (2D) nanoflakes due to their relatively strong atomic bonding in the out-of-plane direction in a crystal system.[21−23] The absence of direct exfoliating methods of 2D transition-metal oxide nanoflakes from layered bulk materials limits the application of such materials. On the other hand, although the size effect of 2D nanoflakes brings high specific surface area and more active site, the poor long-range ion transport as well as the low conductivity led to the unsatisfactory electrochromic performance of α-MoO_3, which must be properly resolved.

In this study, we demonstrated a thiourea-assisted liquid exfoliation strategy for efficiently preparing 2D α-MoO_{3-x} nanoflakes for the first time. By the thiourea addition, the 2D nanoflakes with an average thickness of about 5 nm have been successfully exfoliated under the probe sonication. Then, the 2D nanoflakes were electrophoretically deposited on the transparent indium tin oxide (ITO) glass to achieve the MoO_{3-x} electrochromic film. We further proposed a collaborative tactic to simultaneously enhance the ionic kinetics and boost the structural stability of the MoO_{3-x} film by introducing poly(3,4-ethylenedioxythiophene):poly(styrenesulfonate) (PEDOT:PSS) polymer as the conductive reinforcement. As a result, the prepared MoO_{3-x}/PEDOT:PSS composite film exhibits enhanced electrochromic performance, including improved coloration efficiency, fast switching speed, large transmittance modulation, and enhanced stability. So, we believe that the 2D MoO_{3-x} nanoflakes and their composite materials can open up a new path for the development of cost-effective electrochromic devices.

RESULTS AND DISCUSSION

The main process of liquid-exfoliated MoO_{3-x} nanoflakes starting from bulk α-MoO_3 powder is illustrated in Figure S1, and details can be found in the Experimental Section. The exfoliated MoO_{3-x} nanoflakes were derived from the supernatant after the solution was centrifuged at 5000 rpm for 30 min. To improve the yield of liquid exfoliation of two-dimensional materials, thiourea has been introduced as a functional additive. The content of the Mo element inside the supernatant is related to the exfoliated MoO_{3-x} nanoflakes, which can serve as an indicator of the yield of liquid exfoliation. The results of inductively coupled plasma optical emission spectrometer (ICP/OES) of Mo element are

https://doi.org/10.1021/acsami.4c01108
ACS Appl. Mater. Interfaces 2024, 16, 18052−18062

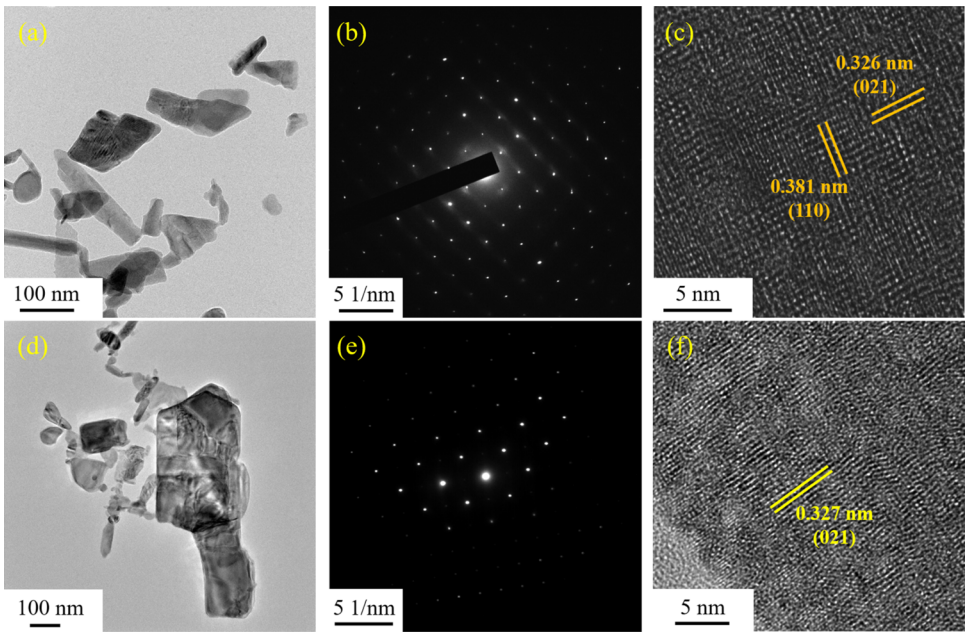

Figure 2. (a) TEM image of the thiourea-assisted exfoliated MoO_{3-x} nanoflakes. (b) SAED image of a thiourea-assisted exfoliated MoO_{3-x} nanoflake. (c) High-resolution transmission electron microscopy (HRTEM) image of a thiourea-assisted exfoliated MoO_{3-x} nanoflake. (d) TEM image of the MoO_{3-x} nanoflakes without thiourea. (e) SAED image of a MoO_{3-x} nanoflake without thiourea. (f) HRTEM image of a MoO_{3-x} nanoflake without thiourea.

measured to verify the efficiency of liquid exfoliation. Figure 1a presents the fluctuation of Mo element content with an error bar between multiple batches of samples. All samples were left to stand for 7 days before testing and the sampling supernatants were taken from different depths below the liquid surface (1, 2, and 3 cm). It can be clearly seen that the largest yield gap of thiourea-assisted exfoliated MoO_{3-x} nanoflakes (2.9 mg mL^{-1}) is about 52.6% higher than that of the pure MoO_{3-x} nanoflakes (1.9 mg mL^{-1}) without thiourea. It means that the efficiency of exfoliating MoO_{3-x} nanoflakes can be improved by thiourea addition. This is because liquid phase exfoliation of MoO_3 with thiourea can be considered as a physical chemistry method. On the one hand, the MoO_3 interlayer spacing can be expanded by the shear force during ultrasonic vibration. On the other hand, oxygen vacancies and sulfur substitution were generated through the chemical reaction between molybdenum oxide and thiourea. This chemical reaction also caused the degeneration of Van der Waals force inside α-MoO_3.[24−28] Owing to the coordination of physical and chemical methods, efficient exfoliation of MoO_3 was ultimately achieved to prepare 2D nanoflakes. Figure 1b is a photograph of the supernatants with or without thiourea addition. The blue color suggests the nonstoichiometric nature of MoO_{3-x} and the existence of oxygen vacancies.[29,30] Obviously, the MoO_{3-x} nanoflakes supernatant of thiourea-assisted exfoliation is deeper blue than the pure MoO_{3-x} nanoflakes supernatant, implying a higher concentration of nanoflakes or more oxygen vacancies (as will be discussed later). Since the thiourea solution is transparent and colorless (Figure S2), it has no effects on the background color. It is worth noting that the significant Tyndall phenomenon can be observed in Figure 1b, which indicates the colloidal property of supernatant.[31] Hence, such a supernatant can be easily electrophoretically deposited onto the ITO transparent electrode to form uniform films.

The atomic force microscopy (AFM) images in Figure 1c,d show the size distribution of exfoliated MoO_{3-x} nanoflakes with and without thiourea. The average thicknesses of the two samples are about 5 and 21 nm, respectively. As the yellow dashed line marked in Figure 1c, the minimal thickness of the thiourea-assisted nanoflake is about 1.6 nm and the lateral size is about 280 nm. Therefore, the exfoliated MoO_{3-x} nanoflakes tend to be a type of two-dimensional material because the thickness of exfoliated MoO_{3-x} nanoflakes could be equivalent to a few atomic layers (planar units of α-MoO_3 are made of atomically thin double layers that have a thickness of about 1.4 nm).[32] As a contrast, Figure 1d shows the size distribution of pure MoO_{3-x} nanoflakes without thiourea; the minimal thickness is about 14 nm. The above results indicate that thiourea is not only beneficial for improving the liquid exfoliation yield but also reduces the thickness of the exfoliated nanoflakes.

To observe the high-resolution morphology and element distribution of thiourea-assisted exfoliated MoO_{3-x} nanoflakes, the results of transmission electron microscopy (TEM) and energy-dispersive spectroscopy (EDS) elemental mapping are further investigated. The morphology of thiourea-assisted exfoliated MoO_{3-x} nanoflakes is presented in Figure 2a, and the selected area electron diffraction (SAED) pattern of a nanoflake is displayed in Figure 2b. It is obvious that the exfoliated nanoflakes tend to be irregular shaped along with major size distribution between 30 and 300 nm, and these results are consistent with previous atomic force microscopy analysis. In addition, the SAED pattern demonstrates the single-crystal nature of the exfoliated nanoflakes. The high-resolution TEM image in Figure 2c exhibits lattice spacing of 0.381 and 0.326 nm, which match well with the (110) and (021) planes (JCPDS No. 35-0609). These results indicate that the thiourea-assisted liquid exfoliation process does not change the crystallography characteristics of the α-phase molybdenum oxide.

https://doi.org/10.1021/acsami.4c01108
ACS Appl. Mater. Interfaces 2024, 16, 18052−18062

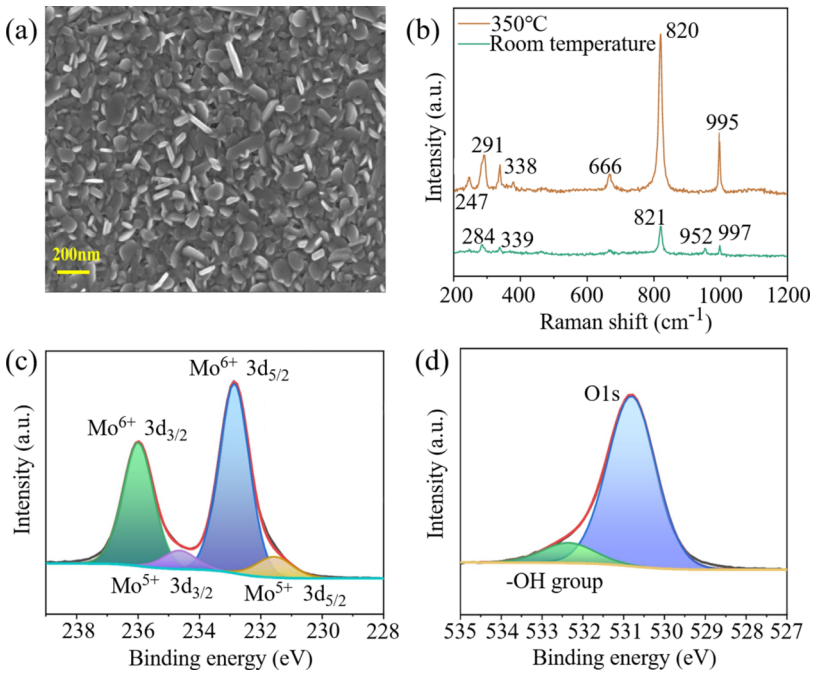

Figure 3. (a) SEM surface image of the electrophoretic-deposited MoO_{3-x} film. (b) Raman spectra of the MoO_{3-x} films dried at room temperature and annealed at 350 °C. (c) X-ray photoelectron spectra (XPS) of the annealed MoO_{3-x} film, Mo 3d scan. (d) XPS spectra of the annealed MoO_{3-x} film, O 1s scan.

The EDS elemental mapping demonstrated in Figure S3a,d clearly reveals that Mo, O, and S elements are uniformly distributed in a single MoO_{3-x} nanoflake. It suggests that monocrystalline MoO_{3-x} nanoflakes have been successfully derived by liquid exfoliation. Thiourea plays an important role during the exfoliating process, as evidenced by the presence of S element in the EDS elemental mapping. The morphology and the selected area electron diffraction (SAED) pattern of exfoliated MoO_{3-x} nanoflakes without thiourea are displayed in Figure 2d,e. It suggests that the exfoliated MoO_{3-x} nanoflakes without thiourea present a single-crystal nature and a larger size, which is consistent with previous results. The high-resolution TEM image in Figure 2f exhibits lattice spacing of 0.327 nm, which matches well with the (021) planes (JCPDS No. 35-0609). The EDS elemental mapping demonstrated in Figure S3e−g clearly reveals that Mo and O elements are uniformly distributed in a single MoO_{3-x} nanoflake.

Next, we fabricated MoO_{3-x} thin films based on thiourea-assisted exfoliated MoO_{3-x} nanoflakes by electrophoretic deposition technology. As shown in Figure S4, a direct current (DC) potential has been applied on the two-electrode system where bare ITO glass and graphite were, respectively, used as the work electrode and counter electrode. Afterward, the deposited MoO_{3-x} films were transferred to a hot plate at 350 °C for about 10 min. Figure 3a shows the scanning electron microscopy (SEM) image of the electrophoretic-deposited MoO_{3-x} film. It can be clearly seen that the MoO_{3-x} film consists of regularly distributed nanoflakes with a main size range from 100 to 300 nm. The result is consistent with previous AFM and TEM analysis data. It is interesting that many nanoflakes are uniformly coated on the ITO substrate by a pattern of stacking during the process of electrophoretic deposition, just as a large number of leaves falling on the ground in autumn. Meanwhile, a few nanoflakes are distributed in an upright or sloping manner. This morphology promotes adequate contact between the MoO_{3-x} nanoflakes and electrolyte and also allows the bottom layer nanoflakes to stack stably on the substrate. Thus, the electrophoretically deposited MoO_{3-x} film is appropriate to fabricate electrochromic devices.

Figure 3b shows a comparison of the Raman spectra of deposited MoO_{3-x} films, which were annealed at 350 °C or dried at room temperature. The sharp peaks in the range from 200 to 1200 cm^{-1} indicate that the corresponding vibrational modes are due to a highly ordered structure. The intrinsic strong peaks at 290, 820, and 995 cm^{-1} are identified in both of the MoO_{3-x} films. The intense Raman band at 820 cm^{-1} (A_g) is a symmetric stretching mode of the terminal oxygen atoms or the doubly connected Mo−O−Mo bridge, which results from corner-shared oxygen. And the 995 cm^{-1} band is the asymmetric stretch of the terminal oxygen atom mode along the *a* and *b* axes, which results from an unshared oxygen, and it is assigned to the layered structure of α-MoO_3.[33−35] Besides, the enlarged Raman peak in the low wavenumber region (from 200 to 400 cm^{-1}) is presented in Figure S5. The 378 cm^{-1} peak is ascribed to O−Mo−O bending and scissoring modes, which become constantly weaker as the layered sheet becomes thinner.[36] It is worth noting that the entire peak positions of both samples are slightly larger owing to more oxygen vacancies, which can exhibit red-shifted absorption edges. On the other hand, the film dried naturally at room temperature appears an extra weak peak at 952 cm^{-1}, because combining the Mo═O stretching mode of substoichiometric MoO_{3-x} and the existence of sectional Mo−S bonds leads to an outcome of $MoO_{3-x}S_y$.[37−39] As a result, the Raman spectrum proves the existence of some substoichiometry in the thiourea-assisted exfoliated nanoflakes, which is due to the intercalation of solvent molecule in the layered α-MoO_3 during the sonication process. Since thiourea is an intrinsic reductant, it can seize some oxygen atoms and eventually cause oxygen vacancies in the nanoflakes.

https://doi.org/10.1021/acsami.4c01108
ACS Appl. Mater. Interfaces 2024, 16, 18052−18062

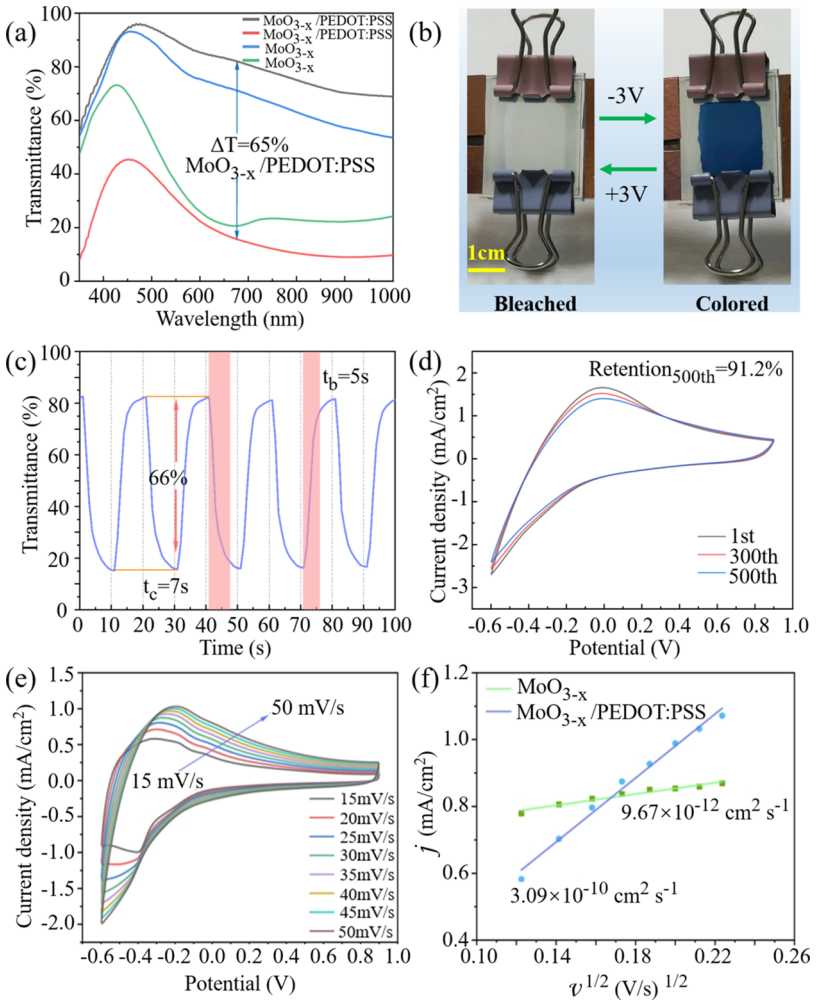

Figure 4. (a) Transmittance spectra of the prepared MoO_{3-x}/PEDOT:PSS and MoO_{3-x} electrochromic devices in colored and bleached states. (b) Photographs of the electrochromic device based on the MoO_{3-x}/PEDOT:PSS film in the bleached state and colored state. (c) *In situ* transmittance curves of the MoO_{3-x}/PEDOT:PSS electrochromic device at 670 nm during the process of coloring (10 s) and bleaching (10 s). (d) Tested cyclic voltammetry (CV) cycling stability of the prepared MoO_{3-x}/PEDOT:PSS film. (e) Cyclic voltammogram curves of the MoO_{3-x}/PEDOT:PSS film at different scan rates range from 15 to 50 mV s^{-1}. (f) Comparison of the functional relationship between peak current density j and the square root of the scan rates $v^{1/2}$ of the prepared MoO_{3-x}/PEDOT:PSS and MoO_{3-x} films.

XPS analysis was also conducted to further validate the substoichiometry of the MoO_{3-x} film made of exfoliated nanoflakes. The XPS survey in Figure S6 shows that there is no existence of impurities or organic species on the surface of the 350 °C annealed MoO_{3-x} film. Figure 3c,d reveals the Mo 3d scan and the O 1s scan XPS spectra of the annealed MoO_{3-x} film. Figure 3c shows that the intense peaks centered at 232.7 and 235.8 eV are attributed to higher oxidation states of Mo^{6+} $3d_{5/2}$ and Mo^{6+} $3d_{3/2}$, respectively.[40] Furthermore, the peaks centered at 234.5 and 231.8 eV are ascribed to Mo^{5+} $3d_{3/2}$ and Mo^{5+} $3d_{5/2}$, respectively, indicating the mixed valence state of Mo^{5+} and Mo^{6+} inside the film.[41] The O 1s spectrum can be deconvoluted into two peaks shown in Figure 3d, and the main peak at 530.8 eV is related to the lattice oxygen in Mo−O chemical species. Another peak that appears at 532.4 eV could be regarded as the surface-adsorbed oxygen contributed by oxygen vacancies and causing unsaturated coordination in Mo atom,[42,43] which is relevant to the −OH group. And the −OH groups are usually bonded to metal cations to maintain the charge balance in substoichiometric oxides. Therefore, the peak intensity of −OH groups can prove the existence of oxygen vacancies.[44,45] As a contrast, Figure S7 reveals XPS spectra of the MoO_{3-x} film dried at room temperature as well as relevant Mo 3d scan, S 2p, and O 1s scan. The XPS survey is similar to the 350 °C annealed MoO_{3-x} film except for the additional S 2p peak. The two S 2p peaks centered at 162.5 and 163.9 eV correspond to S $2p_{3/2}$ and S $2p_{1/2}$, which may be attributed to the partial sulfur atoms participating in Mo−S bonds.[46] Moreover, two extra peaks were found at 165.2 and 165.8 eV that could be considered bridging S_2^{2-} and apical S^{2-} ligands, which indicates the existence of molybdenum sulfide.[47] It is noteworthy that the intensity of all of the low-valence peaks in the Mo 3d scan and OH group in the O 1s scan are obviously stronger than those of the 350 °C annealed MoO_{3-x} film. It means that the MoO_{3-x} films dried at room temperature consisting of exfoliated nanoflakes possessed a large number of oxygen vacancies. Hence, oxygen vacancies existing in the thiourea-assisted exfoliated nanoflakes are generated owing to the ultrasonic power and the reducibility of thiourea. The annealed MoO_{3-x} films still retain some oxygen vacancies, which will improve the electrochromic performance by increasing its electrical conductivity. To demonstrate that thiourea is beneficial for generating oxygen vacancies, the XPS spectra of the exfoliated MoO_{3-x} nanoflakes

https://doi.org/10.1021/acsami.4c01108
ACS Appl. Mater. Interfaces 2024, 16, 18052−18062

without thiourea addition are shown in Figure S8. Based on the calculation of fitting data, the content of Mo^{5+} is approximately 14.5%. As a comparison, the content of Mo_{5+} is about 38.9% in the XPS results of the thiourea-assisted MoO_{3-x} nanoflakes, as shown in Figure S7. Hence, the thiourea-assisted exfoliated MoO_{3-x} nanoflakes have more oxygen vacancies, which agree well with their deeper blue color in Figure 1b.

Next, the annealed MoO_{3-x} film was coated with PEDOT:PSS to form the composite film and assembled into an electrochromic device. To test its electrochromic performance, the transmittance of the MoO_{3-x}/PEDOT:PSS composite film was recorded under oscillating potentials between 3 and −3 V. In addition, MoO_{3-x} film without PEDOT:PSS was also assembled into an electrochromic device following the same procedure for comparison. Figure 4a shows the transmittance spectra of both electrochromic devices. It can be seen that the MoO_{3-x}/PEDOT:PSS device in the bleached state has a high transmittance in the visible to near-infrared wavelength range while it presents a low transmittance in the colored state. Significantly, the transmittance modulation of the MoO_{3-x}/PEDOT:PSS electrochromic device at the wavelength of 670 nm (ΔT = 65%) is far larger than that of the MoO_{3-x} device (ΔT = 51%), which implies that more lithium ions can be injected into the MoO_{3-x}/PEDOT:PSS composite film at the same bias. Figure 4b exhibits photographs of the packaged MoO_{3-x}/PEDOT:PSS electrochromic device in the bleached and colored states. The bleached state is colorless and transparent, while the colored state is deep blue. In addition, the transmittance of the MoO_{3-x}/PEDOT:PSS electrochromic device at 670 nm during the bleaching and coloring process was measured to investigate the dynamic characteristics.

Figure 4c shows the transmittance fluctuates of the device by applying voltages between 3 and −3 V periodically. The stable optical switching with a large transmittance modulation of 66% can be observed in the MoO_{3-x}/PEDOT:PSS electrochromic device with coloring for 10 s and bleaching for 10 s per cycle. The coloring and bleaching response time is defined as the time calculated for 90% transmittance modulation between colored and bleached states. The MoO_{3-x}/PEDOT:PSS electrochromic device presents a fast response with a coloring time (t_c = 7 s) and a bleaching time (t_b = 5 s). As a comparison, the MoO_{3-x} electrochromic device shows a relatively longer coloring time (t_c = 8 s) and bleaching time (t_b = 9 s) while maintaining a smaller transmittance modulation (50%) as shown in Figure S9a. Besides, the coloration efficiency (CE) is another important evaluation factor of electrochromic devices, which can be defined as the changes in optical density (ΔOD) per unit charge density (ΔQ) inserted into or extracted from the electrochromic film per unit area.[48] It can be calculated from the following formula:

$$\mathrm{CE} = \Delta\mathrm{OD}/\Delta Q = \log(T_b/T_c)/\Delta Q \quad (1)$$

where T_b and T_c represent the transmittance of the electrochromic device in the bleached and colored states, respectively. Then ΔQ can be obtained by testing the area of the devices and current integration of the corresponding chronoamperometry curves, as shown in Figures S9b and S10. The calculated CE at 670 nm of the MoO_{3-x}/PEDOT:PSS electrochromic device is about 87.1 $cm^2\ C^{-1}$, which is higher than the value of the MoO_{3-x} electrochromic device (57.3 $cm^2\ C^{-1}$). Moreover, the peak currents in the chronoamperometry curve of the MoO_{3-x}/PEDOT:PSS electrochromic device are obviously higher than that of the MoO_{3-x} electrochromic device. The higher CE and current value indicate more lithium ions, as well as electrons, are extracted and inserted during the coloring and bleaching process,[49] which can be attributed to synergistic benefits of the conductive PEDOT:PSS addition.

In addition, cycling stability is also a very important factor in the electrochromic films in practical applications. Thus, the cyclic voltammetry (CV) curves of electrochromic film have been measured by 500 cycles within the potential range from −0.6 to 0.9 V *vs* the reference electrode. In each cycle, the reversible process of coloring and bleaching can be observed in the MoO_{3-x}/PEDOT:PSS electrochromic film. Figure 4d shows the CV curves for the 1st, 300th, and 500th cycles under the scan rate of 100 mV s^{-1}. As a contrast, the cycling stability of the MoO_{3-x} film has also been tested by the CV curves following the same conditions, as presented in Figure S11a. It can be clearly seen that the closed areas of CV curves in the MoO_{3-x}/PEDOT:PSS film are slightly higher than the MoO_{3-x} film whether the CV curves are 1st or 500th. After 500 cycles, the MoO_{3-x}/PEDOT:PSS film remains at 91.2% of its initial capacity while the MoO_{3-x} film remains at 77.3% of its initial capacity. Compared with that of MoO_{3-x} film, a significantly larger charge retention is found in the MoO_{3-x}/PEDOT:PSS film, which indicates the better cycling stability of the composite. Moreover, cyclic stabilities of the MoO_{3-x}/PEDOT:PSS and MoO_{3-x} electrochromic devices were also presented in Figure S12. After 1000 cycles, the MoO_{3-x}/PEDOT:PSS electrochromic device remains at 67.5% of its initial ΔT while the MoO_{3-x} electrochromic device only remains at 29.6% of its initial ΔT. The stability results of the prepared device after 1000 cycles also prove that the MoO_{3-x}/PEDOT:PSS composite has better long-term tolerance to lithium ions than MoO_{3-x}.

To evaluate the electrochemical behavior of the MoO_{3-x}/PEDOT:PSS film during the bleaching and coloring process, the CV curves were measured at different scan rates. As illustrated in Figure 4e, the CV curves show a similar shape at different scan rates beginning from 15 to 50 mV s^{-1}. The CV curves of the MoO_{3-x} film under the same conditions are presented in Figure S11b. The closed area of each CV curve increases as the scan rate increases, indicating ideal capacitance characteristics. As we can see, the closed areas of CV curves in the MoO_{3-x}/PEDOT:PSS film are slightly larger than that of the MoO_{3-x} film, indicating the enhanced electrochemical behavior in the composite. Figure 4f directly reveals that the peak current density of the prepared MoO_{3-x}/PEDOT:PSS and MoO_{3-x} electrochromic film is a function of $(\text{scan rate})^{1/2}$. Then, the diffusion coefficient (D) of the Li^+ ions can be calculated using the Randles−Sevcik equation as the following formula:[50]

$$j_p = 2.72 \times 10^5 \times D^{1/2} \times n^{3/2} \times C_0 \times v^{1/2} \quad (2)$$

where j_p is the peak current density (mA cm^{-2}), D is the diffusion coefficient in the unit of $cm^2\ s^{-1}$, n is the number of electrons considered to be 1 for Li^+, C_0 is the concentration of electrolyte solution (mol cm^{-3}), and v is the scan rate (V s^{-1}). The calculated diffusion coefficient of lithium ions in the prepared MoO_{3-x}/PEDOT:PSS electrochromic film is about 3.09×10^{-10} $cm^2\ s^{-1}$, while the ion diffusion coefficient in the MoO_{3-x} electrochromic film is about 9.67×10^{-12} $cm^2\ s^{-1}$, as shown in Figure 4f. The R^2 linear fitting result of MoO_{3-x}/PEDOT:PSS film and MoO_{3-x} film is 0.9891 and 0.9619,

https://doi.org/10.1021/acsami.4c01108
ACS Appl. Mater. Interfaces 2024, 16, 18052−18062

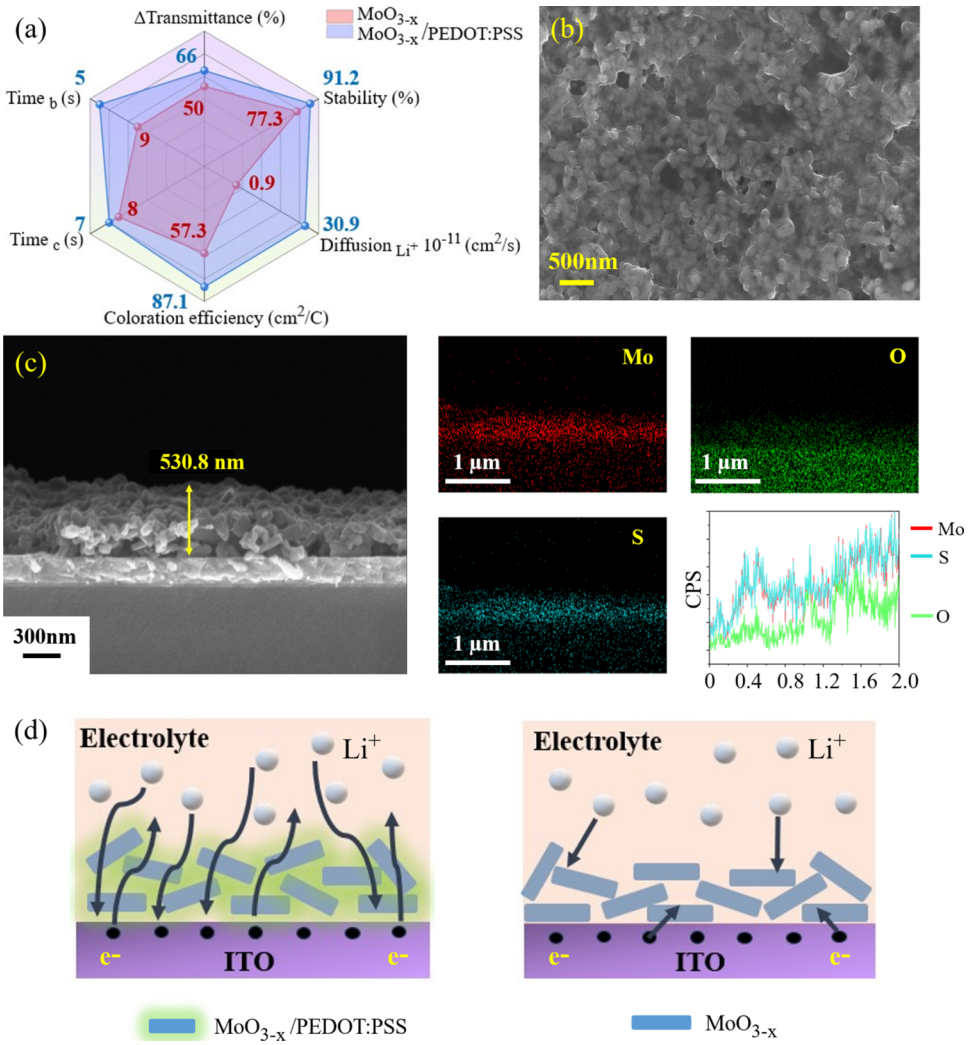

Figure 5. (a) Comparison of the overall electrochromic performance between the MoO_{3-x}/PEDOT:PSS and MoO_{3-x} films. (b) SEM surface image of the MoO_{3-x}/PEDOT:PSS composite film. (c) SEM cross-sectional image and EDS results of the prepared MoO_{3-x}/PEDOT:PSS composite film. (d) A schematic diagram of electron conduction and ion transport on the cross-sectional image of the assembled electrochromic device.

respectively. Thus, the overall ion transport performance of the composite film is better than that of the MoO_{3-x} film. Besides, the electrochemical impedance spectroscopy (EIS) results shown in Figure S13a provide quantized data on the conductivity of the prepared film. The EIS results indicate that the charge transport resistance of the MoO_{3-x}/PEDOT:PSS film is about 33.7 Ω, while the MoO_{3-x} film is about 46.3 Ω. This low resistance value of the prepared MoO_{3-x}/PEDOT:PSS film indicates higher electron conductivity than the MoO_{3-x} film. Moreover, the Bode plots are presented in Figure S13b. The MoO_{3-x}/PEDOT:PSS film exhibits an f_0 of 114.8 Hz, corresponding to a time constant ($\tau_0 = 1/f_0$) of 8.7 ms, which is significantly lower than the 345.3 ms exhibited by the MoO_{3-x} film. The extremely low time constant provides further evidence for the high-speed ion transport inside the MoO_{3-x}/PEDOT:PSS film.[51]

To visually appreciate the improved results, the overall electrochromic index has been directly presented in Figure 5a. The MoO_{3-x}/PEDOT:PSS film shows enhanced electrochromic performance including a large transmittance modulation (ΔT = 65%), a fast switching time (less than 10 s), as well as a large CE of 87.1 cm^2 C^{-1}. All of these parameters exhibit a competitive advantage when compared with those of tungsten oxides or tungsten molybdenum compounds, as shown in Table S1. Figure 5b shows the SEM surface image of the MoO_{3-x}/PEDOT:PSS composite film, while Figure 5c shows the SEM cross-sectional image and EDS mapping results of the composite film. As we can see, the thickness of the prepared MoO_{3-x}/PEDOT:PSS composite film is about 530.8 nm, and also Mo, O, and S elements are uniformly distributed along the thickness direction of the film. It suggests that MoO_{3-x} nanoflakes have been uniformly coated with PEDOT:PSS rather than just on the top of the MoO_{3-x} layer.

As shown in Figure 5a, the performance of the MoO_{3-x}/PEDOT:PSS composite is comprehensively improved compared with the MoO_{3-x} film, especially in terms of charge transport. It can be attributed to the collaborative benefit of multiple factors as follows: (1) PEDOT:PSS is a kind of organic electrochromic material that can demonstrate transmittance modulation ability within the same electrolyte. To figure out the reason for improvement, pure PEDOT:PSS film is used to prepare the electrochromic device and the result is shown in Figure S14. Evidently, the transmittance modulation of pure PEDOT:PSS film at the visible band is better than that

https://doi.org/10.1021/acsami.4c01108
ACS Appl. Mater. Interfaces 2024, 16, 18052−18062

of the near-infrared band. So, the electrochromic effect of PEDOT:PSS is beneficial for the improvement of composite materials in the visible band, but its contribution to the near-infrared band (800−1000 nm) is limited. (2) The boosted ion transport is closely related to the unique nanocomposite structure of MoO_{3-x}/PEDOT:PSS films shown in Figure 5b,c. It can be clearly seen that exfoliated MoO_{3-x} nanoflakes have been successfully covered with the continuous phase PEDOT:PSS. Such a microscopic morphology can effectively make up for the short plate of electrochemical kinetics of 2D MoO_{3-x} nanoflakes. The introduction of PEDOT:PSS is beneficial for long-range ion transport across MoO_{3-x} nanoflakes by providing more channels, resulting in the significantly improved Li^+ ion diffusion coefficient in Figure 5a. (3) As shown in Figure 5d, PEDOT:PSS is able to act as the conductive adhesive, which reduces the resistance of electron conduction inside the MoO_{3-x}/PEDOT:PSS composite. Thanks to the energy-level matching between the two components,[52,53] the participation of electrons in the electrochromic process becomes smoother. In addition, PEDOT:PSS as a polymer can improve the adhesion between MoO_{3-x} nanoflakes and the ITO substrate, promoting the quality of film formation. The problems of film shedding and nanostructure collapsing during long-term cycles will be alleviated, leading to enhanced cycling stability.

CONCLUSIONS

In summary, we creatively fabricated the MoO_{3-x}/PEDOT:PSS inorganic−organic composite film with the aim of high-performance electrochromic devices. The 2D MoO_{3-x} nanoflakes were prepared by a method of thiourea-assisted liquid exfoliation. The experimental results prove that thiourea addition can not only increase the yield of the liquid exfoliation but also reduce the thickness of the nanoflakes. The uniform MoO_{3-x} film obtained through electrophoretic deposition of nanoflakes was further coated with the PEDOT:PSS polymer to simultaneously boost the transport kinetics of electrons and ions. The prepared MoO_{3-x}/PEDOT:PSS composite film shows improved electrochromic performance including large transmittance modulation (65%), large coloration efficiency (87.1 $cm^2\ C^{-1}$), and rapid switching times (t_c = 7 s and t_b = 5 s). In addition, electrochemical measurement results indicate that the MoO_{3-x}/PEDOT:PSS composite significantly boosted ion transport behavior and extended cycle life compared with the MoO_{3-x} component. This work opens the door to develop MoO_{3-x}-based electrochromic materials with improved comprehensive performance, which have potential applications in cost-effective smart windows and other optoelectronic devices.

EXPERIMENTAL SECTION

Materials. All solvents and chemicals were put to use without further purification. Molybdenum trioxide powder (MoO_3, 99.9%) was purchased from Dongming Advanced Material Technology Co., Ltd. Methanol (CH_3OH, 99.5%) and isopropanol (C_3H_8O, 99.5%) were purchased from Meryer Co., Ltd. Thiourea (CH_4N_2S, 99.8%) and ethanol (C_2H_5OH, 99.8%) were purchased from Sinopharm Chemical Reagent Co., Ltd. PEDOT:PSS (KV-ECM-3150) ink was purchased from Zhuhai Kaivo Optoelectronic Technology Co., Ltd. The 1 M $LiClO_4$ electrolyte in a mixed solvent (1:1:1 vol %) of ethylene carbonate (EC)/dimethyl carbonate (DMC)/ethyl methyl carbonate (EMC) was purchased from Dodochem Technology Co., Ltd.

Exfoliation of 2D Nanoflakes. First, 0.12 g of thiourea powder was dissolved in 80 mL of solvents (50 mL of deionized water, 20 mL of methanol, and 10 mL of isopropanol) by continuous magnetic stirring. Meanwhile, 1.44 g of MoO_3 powder was wet ground with 1 mL of deionized water and then dispersed in the previous 80 mL of mixture solution. After stirring at room temperature for 2 h, the above mixture solution was probe sonicated for 5 h. Finally, the exfoliated MoO_{3-x} suspension was centrifuged at 5000 rpm for 30 min to refine the 2D MoO_{3-x} nanoflakes in the supernatant. As a contrast, pure MoO_{3-x} nanoflakes were liquid exfoliated by the same procedure without thiourea addition.

Electrophoretic Deposition of MoO_{3-x} Film. Before the process of electrophoretic deposition, ITO glasses were cleaned with acetone, ethanol, and deionized water in an ultrasonic bath. Then, the MoO_{3-x} films were synthesized via a two-electrode system, in which the bare ITO glass and graphite were used as the work electrode and counter electrode. The liquid-exfoliated MoO_{3-x} nanoflakes were electrophoretically deposited onto the ITO glass at a DC potential of 6 V for 30 s. Subsequently, the wet MoO_{3-x} films were dried at room temperature and transferred to a hot plate at 350 °C for 10 min.

Preparation of MoO_{3-x}/PEDOT:PSS Film and Electrochromic Devices. The conductive PEDOT:PSS ink was dispersed in ethanol with a concentration of 0.3 g mL^{-1}. Then, the PEDOT:PSS solution was spin-coated on the prepared MoO_{3-x} films at a speed of 1000 rpm for 5 s and dried at 100 °C for 15 min. The spin-coating operations were repeated two times to form a MoO_{3-x}/PEDOT:PSS composite film. To fabricate the electrochromic device, the ITO glass with MoO_{3-x}/PEDOT:PSS film, the 1 M $LiClO_4$ electrolyte in a mixed solvent, and another FTO glass were assembled into a sandwich structure and sealed by the transparent silicone.

Characterization. Atomic force microscopy (AFM, Bruker Dimension Icon) was used to characterize the morphology and thickness of the MoO_{3-x} nanoflakes. To carry out the AFM measurement, the silicon tip on a nitride lever probe with ScanAsyst-Air mode was used. The cantilever data are as follows: T = 650 nm, L = 115 μm, f_0 = 70 kHz, k = 0.4 N m^{-1}, and W = 25 μm. High-resolution morphology images of MoO_{3-x} nanoflakes were carried out using a transmission electron microscope (TEM, JEOL JEM-F200). The morphologies of the pure MoO_{3-x} films and MoO_{3-x}/PEDOT:PSS films were recorded by a scanning electron microscope (SEM, ZEISS Gemini 300). The chemical state and valence changes of prepared MoO_{3-x} films were measured by X-ray photoelectron spectroscopy (XPS, Thermo Scientific K-Alpha). Raman results of the prepared MoO_{3-x} films were determined by Raman spectroscopy (Raman, LabRAM HR Evolution) at an excitation wavelength of 532 nm. The content of the Mo element was measured via an inductively coupled plasma optical emission spectrometer (ICP/OES, Agilent 5110). The *in situ* transmittance of electrochromic devices was measured on a spectrophotometer (Mapada V-1600PC) over the wavelength range from 350 to 1000 nm. The chronoamperometry curve was obtained with a digital source meter (Keithley 2410). The cyclic voltammetry (CV) curves were tested with an electrochemical workstation (Zennium Pro, Zahner, Germany) with a three-electrode system. The ITO glass with electrochromic film, graphite sheet, and silver (Ag) wire were used as the work electrode, counter electrode, and reference electrode, respectively. The CV curves were recorded within the potential range from −0.6 to 0.9 V *vs* the reference electrode. Electrochemical impedance spectroscopy (EIS) was also performed on the Zahner impedance analyzer over the frequency range from 100 kHz to 1 mHz, and the alternating current (AC) amplitude was 10.0 mV.

ASSOCIATED CONTENT

Supporting Information

The Supporting Information is available free of charge at https://pubs.acs.org/doi/10.1021/acsami.4c01108.

A schematic diagram presenting the main exfoliation steps from bulk MoO_3 powder to 2D MoO_{3-x}

https://doi.org/10.1021/acsami.4c01108
ACS Appl. Mater. Interfaces 2024, 16, 18052−18062

nanoflakes (Figure S1); photograph of thiourea solution (Figure S2); enlarged morphology of the exfoliated MoO_{3-x} nanoflakes with and without thiourea-assisted and corresponding EDS mapping (Figure S3); a schematic illustration of the electrophoretic deposition to prepare the homogenic MoO_{3-x} film (Figure S4); enlarged Raman spectra of the MoO_{3-x} films in the low wavenumber region range from 200 to 400 cm^{-1} (Figure S5); XPS spectra of the 350 °C annealed MoO_{3-x} film (Figure S6); XPS spectra of the thiourea-assisted MoO_{3-x} film dried at room temperature (Figure S7); XPS spectra of the MoO_{3-x} film dried at room temperature without thiourea (Figure S8); *in situ* optical transmittance curves and corresponding chronoamperometry curve of the prepared MoO_{3-x} electrochromic device at 670 nm (Figure S9); chronoamperometry curve of the MoO_{3-x}/PEDOT:PSS electrochromic device (Figure S10); tested CV cycling stability of the MoO_{3-x} film and CV curves for the MoO_{3-x} film at different scan rates from 15 to 50 mV s^{-1} (Figure S11); cyclic stability of the MoO_{3-x}/PEDOT:PSS and MoO_{3-x} electrochromic devices (Figure S12); electrochemical impedance spectroscopy of the MoO_{3-x}/PEDOT:PSS and MoO_{3-x} including Bode plots of phase angle versus frequency (Figure S13); transmittance spectra of the pure PEDOT:PSS electrochromic device under the coloring and bleaching biases of ±3 V (Figure S14); electrochromic performance of the major tungsten molybdenum oxides (Table S1) (PDF)

AUTHOR INFORMATION

Corresponding Author

Huajing Fang − *Center for Advancing Materials Performance from the Nanoscale (CAMP-Nano), State Key Laboratory for Mechanical Behavior of Materials, Xi'an Jiaotong University, Xi'an 710049, China;* orcid.org/0000-0002-1939-3700; Email: fanghj@xjtu.edu.cn

Authors

Haolin Yu − *Center for Advancing Materials Performance from the Nanoscale (CAMP-Nano), State Key Laboratory for Mechanical Behavior of Materials, Xi'an Jiaotong University, Xi'an 710049, China*

Kai Jing − *Center for Advancing Materials Performance from the Nanoscale (CAMP-Nano), State Key Laboratory for Mechanical Behavior of Materials, Xi'an Jiaotong University, Xi'an 710049, China*

Hailong Ma − *Center for Advancing Materials Performance from the Nanoscale (CAMP-Nano), State Key Laboratory for Mechanical Behavior of Materials, Xi'an Jiaotong University, Xi'an 710049, China*

Lingqi Wu − *Center for Advancing Materials Performance from the Nanoscale (CAMP-Nano), State Key Laboratory for Mechanical Behavior of Materials, Xi'an Jiaotong University, Xi'an 710049, China*

Yang Chai − *Department of Applied Physics, The Hong Kong Polytechnic University, Kowloon, Hong Kong 999077, China;* orcid.org/0000-0002-8943-0861

Complete contact information is available at: https://pubs.acs.org/10.1021/acsami.4c01108

Notes

The authors declare no competing financial interest.

ACKNOWLEDGMENTS

This work was supported by the National Natural Science Foundation of China (No. 51902250) and the Shccig-Qinling Program (2022QL-RQ-CL-002). The authors thank Danli Zhang of the Center for Advancing Materials Performance from the Nanoscale (CAMP-Nano) for contributions to the materials characterization. The Instrument Analysis Center of Xi'an Jiaotong University and Dr. Chao Li are acknowledged for the great help in measurements.

REFERENCES

(1) Wu, W.; Poh, W.; Lv, J.; Chen, S.; Gao, D.; Yu, F.; Wang, H.; Fang, H.; Wang, H.; Lee, P. S. Self-Powered and Light-Adaptable Stretchable Electrochromic Display. *Adv. Energy Mater.* **2023**, *13* (18), 2204103−2204113.

(2) Wang, Z.; Wang, X.; Cong, S.; Geng, F.; Zhao, Z. Fusing electrochromic technology with other advanced technologies: A new roadmap for future development. *Mater. Sci. Eng., R* **2020**, *140*, 100524−100550.

(3) Fang, H.; Zheng, P.; Ma, R.; Xu, C.; Yang, G.; Wang, Q.; Wang, H. Multifunctional hydrogel enables extremely simplified electrochromic devices for smart windows and ionic writing boards. *Mater. Horiz.* **2018**, *5*, 1000−1007.

(4) Cong, S.; Tian, Y.; Li, Q.; Zhao, Z.; Geng, F. Single-Crystalline Tungsten Oxide Quantum Dots for Fast Pseudocapacitor and Electrochromic Applications. *Adv. Mater.* **2014**, *26* (25), 4260−4267.

(5) Zhang, S.; Cao, S.; Zhang, T.; Fisher, A.; Lee, J. Al^{3+} intercalation/de-intercalation-enabled dual-band electrochromic smart windows with a high optical modulation, quick response and long cycle life. *Energy Environ. Sci.* **2018**, *11*, 2884−2892.

(6) Cai, G.; Eh, A.; Ji, L.; Lee, P. S. Recent Advances in Electrochromic Smart Fenestration. *Adv. Sustainable Syst.* **2017**, *1* (12), 1700074−1700097.

(7) Monk, P.; Ali, T.; Partridge, R. The effect of doping electrochromic molybdenum oxide with other metal oxides: Correlation of optical and kinetic properties. *Solid State Ionics* **1995**, *80* (1), 75−85, DOI: 10.1016/0167-2738(95)00130-X.

(8) Liang, Y.; Cao, S.; Wei, Q.; Zeng, R.; Zhao, J.; Li, H.; Yu, W.; Zou, B. Reversible Zn^{2+} Insertion in Tungsten Ion-Activated Titanium Dioxide Nanocrystals for Electrochromic Windows. *Nano-Micro Lett.* **2021**, *13*, 196−208.

(9) Zhao, W.; Wang, J.; Tam, B.; Zhang, H.; Li, F.; Du, A.; Cheng, W. Structural Water in Amorphous Tungsten Oxide Hydrate Enables Fast and Ultrastable Regulation of Near-Infrared Light Transmittance. *Adv. Opt. Mater.* **2023**, *11*, 2202774−2202784.

(10) Wu, W.; Fang, H.; Ma, H.; Wu, L.; Wang, Q.; Wang, H. Self-Powered Rewritable Electrochromic Display based on WO_{3-x} Film with Mechanochemically Synthesized MoO_{3-y} Nanosheets. *ACS Appl. Mater. Interfaces* **2021**, *13*, 20326−20335.

(11) Hsu, C.-S.; Chan, C.; Huang, H.; Peng, C.; Hsu, W. Electrochromic properties of nanocrystalline MoO_3 thin films. *Thin Solid Films* **2008**, *516* (15), 4839−4844.

(12) Wu, W.; Wang, M.; Ma, J.; Cao, Y.; Deng, Y. Electrochromic Metal Oxides: Recent Progress and Prospect. *Adv. Electron. Mater.* **2018**, *4* (8), 1800185−1800203.

(13) Zhang, Y.; Ma, H.; Wu, S.; Yu, H.; Wu, L.; Li, W.; Sun, J.; Wang, H.; Fang, H. Transparent humidity sensor with high sensitivity via a facile and scalable way based on liquid-phase exfoliated MoO_{3-x} nanosheets. *Sens. Actuators Rep.* **2022**, *4*, 100092−100099.

(14) Liang, J.; Sheng, H.; Wang, Q.; Yuan, J.; Zhang, X.; Su, Q.; Xie, E.; Lan, W.; Zhang, C. PEDOT: PSS-glued MoO_3 nanowire network for all-solid-state flexible transparent supercapacitors. *Nanoscale Adv.* **2021**, *3*, 3502−3512.

(15) Ren, H.; Sun, S.; Cui, J.; Li, X. Synthesis, Functional Modifications, and Diversified Applications of Molybdenum Oxides Micro-/Nanocrystals: A Review. *Cryst. Growth Des.* **2018**, *18* (10), 6326−6369.
(16) Yang, Y.; Lau, K.; Zheng, J.; Dong, J.; Wang, L.; Wang, W.; Xu, B.; Qiu, J.; Liu, X. Coupled Femtosecond Laser Assisted Doping and Fragmentation of MoO_3 Nanosheets Generates Plasmonic QDs with Strong NLO Response. *Adv. Opt. Mater.* **2023**, *11* (9), 2202900−2202910.
(17) Kim, H.-S.; Cook, J.; Lin, H.; Ko, J.; Tolbert, S.; Ozolins, V.; Dunn, B. Oxygen vacancies enhance pseudocapacitive charge storage properties of MoO_{3-x}. *Nat. Mater.* **2017**, *16*, 454−460.
(18) Fang, Z.; Liu, C.; Li, X.; Peng, L.; Ding, W.; Guo, X.; Hou, W. Systematic Modification of MoO_3-Based Cathode by the Intercalation Engineering for High-Performance Aqueous Zinc-Ion Batteries. *Adv. Funct. Mater.* **2023**, *33* (7), 2210010−2210023.
(19) Zhang, G.; Xiong, T.; Yan, M.; He, L.; Liao, X.; He, C.; Yin, C.; Zhang, H.; Mai, L. α-MoO_{3-x} by plasma etching with improved capacity and stabilized structure for lithium storage. *Nano Energy* **2018**, *49*, 555−563.
(20) Wang, P.; Chen, Z.; Ji, Z.; Feng, Y.; Wang, J.; Liu, J.; Hu, M.; Wang, H.; Gan, W.; Huang, Y. A flexible aqueous Al ion rechargeable full battery. *Chem. Eng. J.* **2019**, *373* (1), 580−586.
(21) Chhowalla, M.; Liu, Z.; Zhang, H. Two-dimensional transition metal dichalcogenide (TMD) nanosheets. *Chem. Soc. Rev.* **2015**, *44*, 2584−2586.
(22) Song, S. H.; Kim, B.; Choe, D.; Kim, J.; Kim, D.; Lee, D.; Kim, J. M.; Chang, K.; Chang, K. J.; Jeon, S. Bandgap Widening of Phase Quilted, 2D MoS_2 by Oxidative Intercalation. *Adv. Mater.* **2015**, *27* (20), 3152−3158.
(23) Huang, Y.; Sutter, E.; Shi, N.; Zheng, J.; Yang, T.; Englund, D.; Gao, H.; Sutter, P. Reliable Exfoliation of Large-Area High-Quality Flakes of Graphene and Other Two-Dimensional Materials. *ACS Nano* **2015**, *9* (11), 10612−10620.
(24) Sarkar, D.; Das, D.; Das, S.; Kumar, A.; Patil, S.; Nanda, K.; Sarma, D.; Shukla, A. Expanding Interlayer Spacing in MoS_2 for Realizing an Advanced Supercapacitor. *ACS Energy Lett.* **2019**, *4*, 1602−1609.
(25) Shu, Y.; Zhang, W.; Cai, H.; Yang, Y.; Yu, X.; Gao, Q. Expanding the interlayers of molybdenum disulfide toward the highly sensitive sensing of hydrogen peroxide. *Nanoscale* **2019**, *11*, 6644−6653.
(26) Phalswal, P.; Gadhok, M.; Khanna, P. Microwave mediated synthesis of layered MoS_2 nanostructures and its conversion to MoO_3 nanoparticles. *Inorg. Chem. Commun.* **2023**, *153*, 110737−110740.
(27) Sánchez-Salas, R.; Munoz-Sandoval, E.; Endo, M.; Morelos-Gómez, A.; López-Urías, F. Nitrogen and Sulfur Incorporation into Graphene Oxide by Mechanical Process. *Adv. Eng. Mater.* **2021**, *23*, 2001444−2001458.
(28) Shomalian, K.; Bagheri-Mohagheghi, M.; Ardyanian, M. Characterization and study of reduction and sulfurization processing in phase transition from molybdenum oxide (MoO_2) to molybdenum disulfide (MoS_2) chalcogenide semiconductor nanoparticles prepared by one-stage chemical reduction method. *Appl. Phys. A: Mater. Sci. Process.* **2017**, *123*, 93−100.
(29) Li, Y.; Cheng, J.; Liu, Y.; Liu, P.; Cao, W.; He, T.; Chen, R.; Tang, Z. Manipulation of Surface Plasmon Resonance in Sub-Stoichiometry Molybdenum Oxide Nanodots through Charge Carrier Control Technique. *J. Phys. Chem. C* **2017**, *121* (9), 5208−5214.
(30) Cong, S.; Geng, F.; Zhao, Z. Tungsten Oxide Materials for Optoelectronic Applications. *Adv. Mater.* **2016**, *28* (47), 10518−10528.
(31) Jiang, Y.; Wu, Z.; Jiang, L.; Pan, Z.; Yang, P.; Tian, W.; Hu, L. Freestanding $CoSeO_3{\cdot}H_2O$ nanoribbon/carbon nanotube composite paper for 2.4 V high-voltage, flexible, solid-state supercapacitors. *Nanoscale* **2018**, *10*, 12003−12010.
(32) Alsaif, M. M. Y. A.; Latham, K.; Field, M.; Yao, D.; Medehkar, N.; Beane, G.; Kaner, R.; Russo, S.; Ou, J.; Zadeh, K. Tunable Plasmon Resonances in Two-Dimensional Molybdenum Oxide Nanoflakes. *Adv. Mater.* **2014**, *26* (23), 3931−3937.
(33) Ji, F.; Ren, X.; Zheng, X.; Liu, Y.; Pang, L.; Jiang, J.; Liu, S. 2D-MoO_3 nanosheets for superior gas sensors. *Nanoscale* **2016**, *8*, 8696−8703.
(34) Dwivedi, C.; Mohammad, T.; Bharti, V.; Patra, A.; Pathak, S.; Dutta, V. CoSP approach for the synthesis of blue MoO_3 nanoparticles for application as hole transport layer (HTL) in organic solar cells. *Sol. Energy* **2018**, *162* (1), 78−83.
(35) Jittiarporn, P.; Sikong, L.; Kooptarnond, K.; Taweepreda, W.; Stoenescu, S.; Badilescu, S.; Truong, V. Electrochromic properties of MoO_3-WO_3 thin films prepared by a sol-gel method, in the presence of a triblock copolymer template. *Surf. Coat. Technol.* **2017**, *327* (25), 66−74.
(36) Chithambararaj, A.; Bose, A. Investigation on structural, thermal, optical and sensing properties of meta-stable hexagonal MoO_3 nanocrystals of one-dimensional structure. *Beilstein J. Nanotechnol.* **2011**, *2*, 585−592.
(37) Liu, H.; Cai, Y.; Han, M.; Guo, S.; Lin, M.; Zhao, M.; Zhang, Y.; Chi, D. Aqueous and mechanical exfoliation, unique properties, and theoretical understanding of MoO_3 nanosheets made from free-standing α-MoO_3 crystals: Raman mode softening and absorption edge blue shift. *Nano Res.* **2018**, *11*, 1193−1203.
(38) Alsaif, M. M. Y. A.; Field, M.; Daeneke, T.; Chrimes, A.; Zhang, W.; Carey, B.; Berean, K.; Walia, S.; Embden, J.; Zhang, B.; Latham, K.; Kalantar-zadeh, K.; Ou, J. Exfoliation Solvent Dependent Plasmon Resonances in Two-Dimensional Sub-Stoichiometric Molybdenum Oxide Nanoflakes. *ACS Appl. Mater. Interfaces* **2016**, *8* (5), 3482−3493.
(39) Alsaif, M. M. Y. A.; Field, M.; Murdoch, B.; Daeneke, T.; Latham, K.; Chrimes, A.; Zoolfakar, A.; Russo, S.; Ou, J.; Kalantar-zadeh, K. Substoichiometric two-dimensional molybdenum oxide flakes: a plasmonic gas sensing platform. *Nanoscale* **2014**, *6*, 12780−12791.
(40) Yu, M.; Shao, H.; Wang, G.; Yang, F.; Liang, C.; Rozier, P.; Wang, C.; Lu, X.; Simon, P.; Feng, X. Interlayer gap widened α-phase molybdenum trioxide as high-rate anodes for dual-ion-intercalation energy storage devices. *Nat. Commun.* **2020**, *11*, No. 1348, DOI: 10.1038/s41467-020-15216-w.
(41) Li, N.; Li, Y.; Sun, G.; Ma, Y.; Chang, T.; Ji, S.; Yao, H.; Cao, X.; Bao, S.; Jin, P. Selective and Tunable Near-Infrared and Visible Light Transmittance of MoO_{3-x} Nanocomposites with Different Crystallinity. *Chem. Asian J.* **2017**, *12* (14), 1709−1714.
(42) Shen, S.; Zhang, X.; Cheng, X.; Xu, Y.; Zhou, X.; Huo, L.; et al. Oxygen-Vacancy-Enriched Porous α-MoO_3 Nanosheets for Trimethylamine Sensing. *ACS Appl. Nano Mater.* **2019**, *2* (12), 8016−8026.
(43) Etman, A. S.; Abdelhamid, H.; Yuan, Y.; Wang, L.; Zou, X.; Sun, J. Facile Water-Based Strategy for Synthesizing MoO_{3-x} Nanosheets: Efficient Visible Light Photocatalysts for Dye Degradation. *ACS Omega* **2018**, *3* (2), 2193−2201.
(44) Rahimnejad, S.; He, J.; Chen, W.; Wu, K.; Xu, G. Tuning the electronic and structural properties of WO_3 nanocrystals by varying transition metal tungstate precursors. *RSC Adv.* **2014**, *4*, 62423−62429.
(45) Zhuiykov, S.; Kats, E.; Carey, B.; Balendhran, S. Proton intercalated two-dimensional WO_3 nano-flakes with enhanced charge-carrier mobility at room temperature. *Nanoscale* **2014**, *6*, 15029−15036.
(46) Sygellou, L. An in-situ photoelectron spectroscopy study of the thermal processing of ammonium tetrathiomolybdate, $(NH_4)_2MoS_4$ precursor. *Appl. Surf. Sci.* **2019**, *476* (15), 1079−1085.
(47) Noori, Y. J.; Thomas, S.; Ramadan, S.; E Smith, D.; K Greenacre, V.; Abdelazim, N.; Han, Y.; Beanland, R.; L Hector, A.; Klein, N.; Reid, G.; N Bartlett, P.; Groot, C. H. Large-Area Electrodeposition of Few-Layer MoS_2 on Graphene for 2D Material Heterostructures. *ACS Appl. Mater. Interfaces* **2020**, *12*, 49786−49794.
(48) Zhou, J.; Wei, Y.; Luo, G.; Zheng, J.; Xu, C. Electrochromic properties of vertically aligned Ni-doped WO_3 nanostructure films

and their application in complementary electrochromic devices. *J. Mater. Chem. C* **2016**, *4*, 1613−1622.
(49) Ling, H.; Liu, L.; Lee, P.; Mandler, D.; Lu, X. Layer-by-Layer Assembly of PEDOT: PSS and WO_3 Nanoparticles: Enhanced Electrochromic Coloration Efficiency and Mechanism Studies by Scanning Electrochemical Microscopy. *Electrochim. Acta* **2015**, *174* (20), 57−65.
(50) Wu, W.; Fang, H.; Ma, H.; Wu, L.; Zhang, W.; Wang, H. Boosting Transport Kinetics of Ions and Electrons Simultaneously by $Ti_3C_2T_x$ (MXene) Addition for Enhanced Electrochromic Performance. *Nano-Micro Lett.* **2021**, *13*, 20−33.
(51) Shao, Y.; Elkady, M.; Lin, C.; Zhu, J.; Marsh, K.; Hwang, J.; Zhang, Q.; Li, Y.; Wang, H.; Kaner, R. 3D Freeze-Casting of Cellular Graphene Films for Ultrahigh-Power-Density Supercapacitor. *Adv. Mater.* **2016**, *28*, 6719−6726.
(52) Jung, S.; Junghyun, L.; Ungsoo, K.; Hyesung, P. Solution-Processed Molybdenum Oxide with Hydroxyl Radical-Induced Oxygen Vacancy as an Efficient and Stable Interfacial Layer for Organic Solar Cells. *Sol. RRL* **2020**, *4* (3), 1900420−1900430.
(53) Lee, M.-H.; Chen, L.; Li, N.; Zhu, F. MoO_3-induced oxidation doping of PEDOT: PSS for high performance full-solution-processed inverted quantum-dot light emitting diodes. *J. Mater. Chem. C* **2017**, *5*, 10555−10561.

https://doi.org/10.1021/acsami.4c01108
ACS Appl. Mater. Interfaces 2024, 16, 18052−18062